KATRIN ADLER
TU-Bergakademie Freiberg, Deutschland
Institut für Mechanik und Fluiddynamik,
e-mail: katrin.adler@imfd.tu-freiberg.de
LESZEK BLACHA
Politechnika Śląska, Katedra Metalurgii
ul. Krasińskiego 8, 40-019 Katowice
e-mail: Leszek.Blacha@polsl.pl
VLADIMIR GALINDO
Forschungszentrum Roßendorf, Dresden, Deutschland
Abteilung für Magnetohydrodynamik
REUDIGER SCHWARZE
TU-Bergakademie Freiberg, Deutschland
Institut für Mechanik und Fluiddynamik,
e-mail: Ruediger.Schwarze@imfd.tu-freiberg.de

UKD 669.181.274 : 519.6 : 536.24 : 532.517.4

Determination of value of mass transfer coefficient electromagnetic stirred liquid metal phase

Wyznaczanie wartości współczynnika wnikania masy w ciekłej fazie metalowej mieszanej indukcyjnie

The paper presents the method of determination of mass transfer coefficient in electromagnetic stirred liquid phase based on Lamont, Scott and Kolmogorov turbulent models. For this purpose the numerical model allowing the determination of electromagnetic force and turbulent field was utilized. As result the values of Lorentz forces and metal surface velocity have been determined. Calculations were made for IS5/III Leybold Heraeus induction furnace.

Piece indukcyjne należą do tych urządzeń, które od lat wykorzystywane są do wytopu różnych gatunków stali. W procesach występuje wiele zjawisk fizykochemicznych, zachodzących w układzie ciekła faza metaliczna-faza gazowa. Wspomnieć tu należy np. o odparowaniu lotnych składników kąpieli lub desorpcji gazów rozpuszczonych w ciekłym metalu. Z kinetycznego punktu widzenia o szybkości tych zjawisk decydują m.in. zjawiska transportu masy w obu fazach. Charakter ruchu i jego intensywność, wywołany działaniem sił pola elektromagnetycznego, są funkcjami wielu zmiennych, takich jak geometria pieca, gęstość wydzielanej mocy, częstotliwość, a także usytuowanie wzbudnika względem metalicznego wsadu. W prezentowanym artykule przedstawiono metodę wyznaczania wartości współczynnika wnikania masy w ciekłej fazie mieszanej indukcyjnie, z wykorzystaniem modeli turbulentnych Lamonta i Scotta, a także Kolmogorova. Wykorzystano do tego model numeryczny, pozwalający na określenie pola sił elektromagnetycznych i pola turbulencji. Dzięki temu wyznaczono wartości sił Lorentza, a następnie określono prędkość przypowierzchniową metalu. Obliczenia wykonano dla próżniowego pieca indukcyjnego IS5/III firmy Leybold Heraeus. Znajomość wartości współczynnika wnikania masy w ciekłej fazie metalicznej mieszanej indukcyjnie może pozwolić na opis zjawisk zachodzących w wielu procesach metalurgicznych, m.in. w procesach wytopu i obróbki próżniowej stali.

Keywords: mass transfer coefficient, electromagnetic stirred molten metal, numerical simulation, turbulent flow, induction furnaces

Słowa kluczowe: *współczynnik wnikania masy, elektromagnetyczne mieszanie ciekłej kąpieli metalowej, modelowanie numeryczne, przepływy burzliwe, piece indukcyjne*

1. **Introduction.** The melting processes in induction vacuum furnaces are applied mainly in production of special steel grades. This is related to heat resisting steels, tool steels, transformer and stainless steels, and also so called magnetic alloys. This technology also has found an application in metallurgy of non-ferrous metals used for the production of high purity metals and their alloys.

The characteristic features of the metal and alloy melting processes in induction vacuum furnaces can be described as follows:

- thanks to the execution of metallurgical processes in enclosed chambers connected to a system of vacuum pumps, it is possible to obtain practically any chemical composition of gaseous phase within a very wide pressure range. This means, that the whole system of this phase can be accurately controlled according to technological assumptions of the process,
- a possibility to run the metallurgical process practically without slagging phase and in optional atmosphere allows for a safe prolonged holding of the bath in the unit until achieving appropriately low level of gas content, metallic or non-metallic impurities,
- induction heating with a possibility of frequency modulation of supply current is causing very intensive stirring of bath. This has a very positive effect on the speed of a number of chemical reactions taking place during performed melting process, and has effect on homogenization of the bath composition. The latter is especially important at introduction of alloy additives.

As mentioned before, in the melting process of metals and alloys in induction vacuum furnaces there exists a possibility for removal of volatile metallic impurities from the bath. This removal is realized by evaporation of impurities. Taking into consideration

the importance of evaporation effect in many metallurgical processes, as well as its complicity because of heterogeneous character, the recognition of its kinetics is the aim of research by metallurgists since many years. These examinations mainly cover the determination of the influence of pressure, temperature, composition of metal bath or hydrodynamics of adopted metallurgical units on the rate of evaporation process. This allows to determine the stages defining the process rate.

2. **Kinetic of evaporation process.** It is known that analyzed process of evaporation has a heterogeneous character and takes place in the system of liquid metal–gaseous phase. It is a multistage process where the following steps can be defined:

1. mass transfer of evaporating agent from inside of liquid metal to interfacial boundary (mass transfer in liquid phase),
2. evaporation of component from interfacial surface (physical transformation at interfacial surface, here a facial transition from the liquid into gaseous state),
3. mass transfer of evaporating component from interfacial surface into the gaseous phase (mass transfer in gaseous phase).

The mass transfer coefficient in an evaporation process can be defined by a general equation:

$$\frac{1}{k} = \frac{1}{\beta_L} + \frac{1}{k_e} + \frac{1}{\beta_g} \tag{1}$$

where: β_L, β_g – mass transfer in liquid and gaseous phase, $\mathrm{m \cdot s^{-1}}$,
k_e – the rate of evaporation constant, $\mathrm{m \cdot s^{-1}}$.

According to equation (1) it is necessary to know the values of β_L, β_g and k_e to define the value of the mass transfer coefficient k.

In order to determine the value of the mass transfer coefficient in liquid alloys during induction stirring the Machlin's model, based on penetration models of mass transfer [1] is mostly used. According to this model, the mass transfer coefficient is defined by the relation:

$$\beta_L = \left(\frac{8 D_{AB} v_m}{\Pi r_m} \right)^{0.5} \tag{2}$$

where: D_{AB} – coefficient of diffusion A-component in B-component, $\mathrm{m^2 s^{-1}}$,
v_m – velocity of flow to interface, $\mathrm{m \cdot s^{-1}}$,
r_m – radius of metal bath, m.

This relationship is based on the assumption that the bath is being shifted as rigid body along the surface of contact between bath-gas and bath-crucible. According to Machlin, the speed vm slightly depends on electric parameters of the furnace, as well as its size. It was assumed that for the determination of β_L from relation (2) for the units with a capacity up to 1 t of liquid metal the value of v_m is constant at a value of $0.1\ \mathrm{ms^{-1}}$.

The misrepresentation of constant near-surface speed of metal with induction stirring made by Machlin was disclosed by examinations performed under supervision of Szekely, Tarapore and Evans [2÷5]. They executed, among others, the experimental measurements of metal flow rate under induction stirring and have proved its variability depending on electrical parameters of the furnace and on geometrical dimensions of the adopted unit.

Another relation defining the mass transfer coefficient in induction stirred metallic bath is presented the work [6]. It has the form:

$$\beta_L = 2.55 \cdot 10^{-4} \left(\frac{F}{V} \cdot f \right)^{0.25} T \cdot r_m^{0.5} \cdot D_{AB}^{0.5} \tag{3}$$

where: r – radius of metal bath, m,
F – surface of evaporation, $\mathrm{m^2}$,
V – volume of liquid metal, $\mathrm{m^3}$.

We know, that the mass transfer at the interface of an electromagnetically stirred molten metal is strongly influenced by the turbulent flow near this interface [6]. As a consequence the liquid-side mass transfer coefficient β_L can be deduced from characteristic scales of turbulence [7]. Here, two different eddy-structure models will be employed in order to approximate β_L. These models imply the identification of a surface renewal time scale τ governing the mass transfer.

The mass transfer at the interface is also controlled by molecular diffusion. Hence, to calculate the mass transfer coefficient for the liquid phase the following equation will be used:

$$\beta_L = C \sqrt{\frac{D_{AB}}{\tau}} \tag{4}$$

The variable τ denotes a characteristic time scale of the turbulence as mentioned above. The first eddy-structure model identifies τ as the turnover time of the large scale turbulent eddies:

$$\tau = \frac{\Gamma}{U_{ch}} \tag{5}$$

where: Γ is a characteristic length of large scale turbulence,
U_{ch} is a characteristic velocity.

According to the k-ε model which will be implemented here, $U_{ch} = k^{1/2}$ and a characteristic length corresponds to $\Gamma = k^{3/2} \cdot \varepsilon^{-1}$. Hence, the characteristic time scale is $\tau_1 = k \cdot \varepsilon^{-1}$. The values for k, the turbulent kinetic energy, and for ε, the turbulent dissipation rate, can be taken from the results of the numerical calculation. The value for the constant is set at $C = 0.5$ due to the proposal of Lamont and Scott [9]. Hence, the mass transfer rate β_{L1} can be calculated by the following equation:

$$\beta_{L1} = 0.5 \sqrt{\frac{D_{AB} \cdot \varepsilon}{k}} \tag{6}$$

The second eddy-structure model identifies τ as the Kolmogorov time scale which is the turnover time of the smallest turbulent eddies in the flow: $\tau_2 = \sqrt{\eta / \rho \cdot \varepsilon}$. This model describes the mass transfer at the liquid-gas interface according to the turbulent surface renewal theory by Lamont and Scott [9]. Therefore, β_{L2} is calculated by

$$\beta_{L2} = 0.5 \frac{(D_{AB}^{1/2})}{(\eta / \rho \cdot \varepsilon)^{1/4}} \tag{7}$$

3. Calculation of turbulent mass transfer coefficient

3.1. *Physical basics.* Figure 1 shows the set-up with the crucible and the coil schematically. All physical values which are important for the calculation of the magnetic field and the flow field are given in table 1.

The wave length of the magnetic field is large compared to the radius $r_a = 0.041$ m of the crucible. Hence, displacement currents within the melt are neglected.

Because of the frequency (3 kHz) of the magnetic field it is treated as quasi-static. It is also assumed that the magnetic field is not influenced by the flow field.

3.2. *Basic equations.* The Maxwell equations of the quasi-static magnetic field reduce to the diffusion equation of the magnetic vector potential $\vec{A}$:

$$\frac{1}{\mu}\frac{\partial^2 A_i}{\partial x_j^2} = \sigma\frac{\partial A_i}{\partial t} + j_{S,i} \tag{8}$$

A_i and $j_{S,i}$ are the components of $\vec{A}$ and the coil current density $\vec{j}$, respectively. The Lorentz force density $\vec{f}_L$ which is deduced from the magnetic vector potential is added as a source term to the Reynolds-averaged Navier-Stokes equations:

$$\rho\overline{u_i}\frac{\partial\overline{u_i}}{\partial x_j} = \frac{\partial\overline{p}}{\partial x_i} + (\eta + \eta_t)\frac{\partial^2\overline{u_i}}{\partial x_j^2} + \overline{f_{L,i}} \tag{9}$$

Here $\overline{u_i}$ and $\overline{f_{L,i}}$ are the components of the velocity and the Lorentz force vector, respectively. The variable $\overline{p}$ denotes the pressure, ρ is the density, η the viscosity of the melt given in table 1 and η_t is the turbulent viscosity. The continuity equation completes the description of the problem:

$$\frac{\partial\overline{u_i}}{\partial x_i} = 0 \tag{10}$$

3.3. *Turbulence model.* The turbulent viscosity in equation (9) needs to be modeled. In absence of any validated model specific for closed MHD flows, three different turbulence models are tested here. The two-equation *RNG-k-ε* model is employed first. Its use is based on the experience that this model works well for a large variety of flow simulations [10, 11]. Later on the Reynolds Stress Model (RSM) and the k-ω model will be tested as well.

3.4. *Boundary conditions.* The flow is assumed to be axisymmetric. Hence, a two-dimensional, axisymmetric, structured grid with 2652 cells (39 cells in the radial direction, 68 cells in the axial direction) will be used. The model includes two walls at which the no-slip condition is applied, the bottom of the crucible and its side wall. The grid is refined near the side wall in order to resolve higher velocity and force gradients. For the surface of the crucible a wall boundary condition with specified shear of zero is employed to simulate the free surface. Non-equilibrium wall functions are used to calculate the turbulent flow near the walls.

3.5. *Calculation of the magnetic field and the flow field.* The magnetic field is calculated using the commercial software OPERA. The Lorentz force which is generated by the magnetic field is then stored for discrete grid coordinates.

The flow field is calculated using the commercial CFD software FLUENT. The grid coordinates for the flow calculation are identical to the coordinates of the grid for the magnetic field calculation. This is advantageous since the Lorentz force does not have to be interpolated on a different grid and deviations of the force field between both calculations can be excluded. A User Defined Function (UDF) is employed in order to initialize the flow field with the Lorentz force.

QUICK is used as discretization scheme for the convective terms of equation (9) and for the turbulence equations [12]. The diffusive term in equation (9) is discretized with the central differencing scheme. The Rhie and Chow method [13] is employed for the pressure interpolation and for the pressure-velocity coupling the PISO method [14] is used.

4. Results

4.1. *The magnetic field and the flow field.* Due to the skin effect, the Lorentz force acts mainly near the wall of the crucible, see figure 2. The maximum force density is $f_L = 40\,000$ N m^{-3} and occurs at the bottom and the top of the crucible. The penetration depth δ of the Lorentz force in the melt can be calculated by the following equation:

$$\delta = \sqrt{\frac{2}{\mu\sigma\omega}} \tag{11}$$

The values for μ and σ are given in table 1, $\omega = 18.8$ kHz is the angular frequency of the magne-

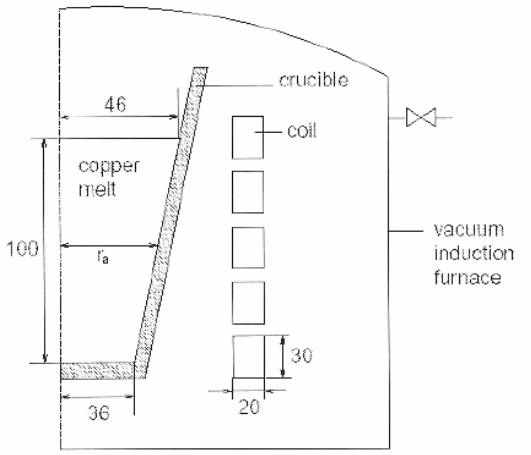

Fig. 1. Sketch of the vacuum induction unit, lengths are given in mm
Rys. 1. Schemat indukcyjnego pieca próżniowego, wymiary w mm

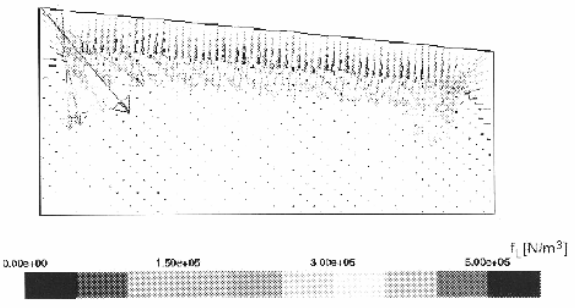

Fig 2. Lorentz force density vector, geometry rotated left by 90°
Rys. 2. Rozkład sił Lorentza, geometria obrót 90° w lewo

Table 1. Physical quantities of the melt
Tablica 1. Parametry fizyczne metalu

Quantity	Symbol	Value
Magnetic permeability	μ	$1.257 \cdot 10^{-6}$, H m^{-1}
Electrical conductivity	σ	$4 \cdot 10^6$, S m^{-1}
Density	ρ	7.9, Mg m^{-3}
Viscosity	η	0.0015 Pa · s
Frequency	f	3000 Hz

tic field which gives $\delta = 4.59$ mm. Consequently the grid needs to be refined near the wall to resolve the force gradient and the velocity gradients later on as already mentioned.

As assumed before the flow is characterized by two counter-rotating vortex rings which are shown in figure 3. However at the side-wall between the upper and lower vortex there is another small vortex. It can be seen that the appearance of this vortex depends strongly on the use of the turbulence model, i.e. it changes its position and shape, respectively. In corresponding experiments no evidence for such a vortex is found. Therefore this small vortex seems to be a numerical error.

The most reliable result seems to be yielded with the *RNG-k-ε* model. Here the extension of additional structures remains the smallest. Hence this model will be used for further investigations concerning the mass transfer rates.

The velocity magnitudes of the vector plot shown in figure 4 are similar for all turbulence models investigated here. The maximum velocity which is marked by the long arrows occurs near the wall of the crucible in accordance to the maximum Lorentz force. The results of the simulation runs shown in figures 3 and 4 were achieved at a coil current of $I = 992$ A. The maximum velocity is 0.308 m s^{-1}. This value is very close to the Alfven velocity which is $u_A = 0.357$ m s^{-1} for this configuration presented above. However the magnitude of the coil current implies an uncertainty in the present investigation. Due to this fact, the flow is simulated for different coil currents and the results for the maximum velocity and the mass transfer rates will be compared with each other, respectively. In table 2 the maximum velocities and the corresponding Alfven velocities for different coil currents are summarized. As one can see there are only little deviations between both velocities. The maximum flow velocity is always slightly below the Alfven velocity.

4.2. *The mass transfer coefficient.* From the flow data, the values for the turbulent kinetic energy and the dissipation rate were calculated as area weighted mean values. The values were determined 2 mm below the free surface in order to exclude false data due to the influence of the boundary conditions for the free surface. The time scales τ_1 and τ_2 as well as the evaporation rates β_L were obtained according to the eddy structure models. The results for the transfer coefficient β_L, which were determined according to equation (6) and (7) are presented in figure 5, respectively.

We found that the numerical simulation of the flow fields at coil currents lower than 500 A is difficult. Strongly opposed criteria due to the turbulence modelling on the one hand and due to action of the Lorentz force on the other hand exists. Therefore, additional simulations which were run at higher coil currents, where we were not in trouble with these

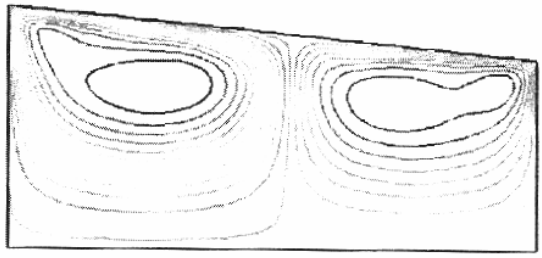

(a) $RNG - k - \epsilon$ model

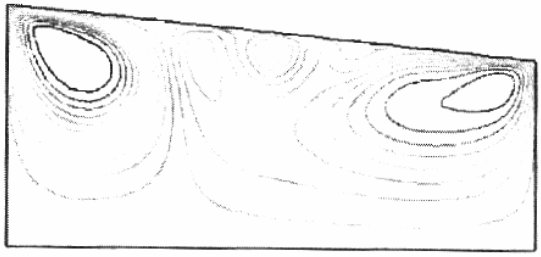

(b) Reynolds Stress model

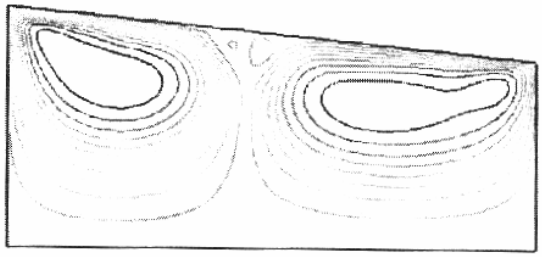

(c) $k - \omega$ model

Fig. 3. Stream function, models rotated left by 90°
Rys. 3. Zmiany strumienia, geometria obrót 90° w lewo

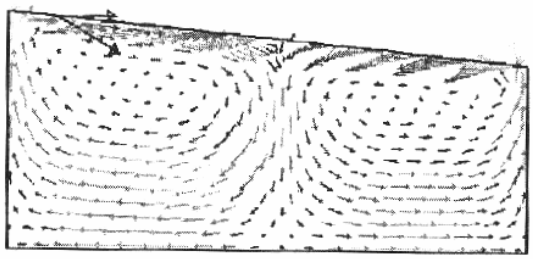

Fig. 4. Velocity vectors of the flow field
Rys. 4. Wektory prędkości pola przepływów

Table 2. Flux density and Alfven velocities for different currents
Tabela 2. Wartości gęstości strumienia i prędkości dla różnych wartości natężenia prądu

Current I, A	155	248	496	992	1526	1984
Flux density B_o, T	0.0056	0.0089	0.018	0.036	0.055	0.071
Alfven vel. u_a, m s^{-1}	0.056	0.089	0.179	0.357	0.55	0.714
max. flow vel. u_{max}	0.037	0.065	0.141	0.308	0.449	0.618

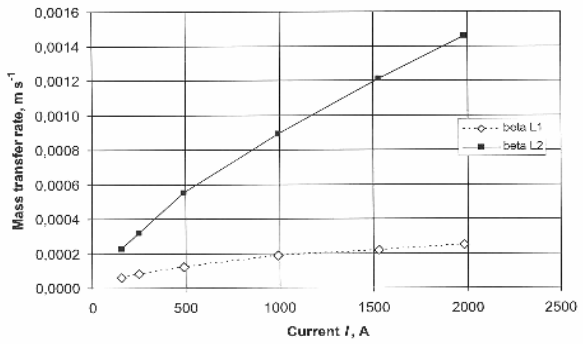

Fig. 5. Mass transfer rates as function of the current
Rys. 5. Współczynnik wnikania masy w funkcji natężenia prądu

criteria. Figure 5 gives a reasonable prediction of the liquid side mass transfer coefficient. It is possible to estimate the uncertainty in β_{L1} and β_{L2} from their slopes, respectively. It can also be assumed that both time scales τ_1 and τ_2 influence the liquid side mass transfer. Hence it can be expected that the correct mass transfer coefficient will be located somewhere between β_{L1} and β_{L2}.

5. **Conclusion.** The paper presents a new method for the calculation of the liquid mass transfer coefficient of an electromagnetically stirred molten metal. For this purpose, at first the magnetic field is determined, next the turbulent flow field is calculated and finally the turbulent mass transfer coefficient is estimated from the turbulence quantities. Two different approaches are employed in order to estimate this coefficient. It can be assumed that the correct mass transfer coefficient will be located somewhere between these two estimates.

References

1. *Bakish B., Winkler O.:* Vacuum Metallurgy, Elsevier Amsterdam 1971

2. *Szekely J., Chang W.:* Iron and Steelmaking, vol. 3, 1977, p. 196–204

3. *Tarapore E. D., Evans J. W.:* Metall. Trasn. B, vol. 7B, 1976, p. 343–351

4. *Tarapore E. D., Evans J. W., Langfeld J.:* Metall. Trasn. B, vol. 8B, 1977, p. 179–184

5. *Chang C. W., Szekely J., Eagar T. W.:* "The analysis of magnetohydrodynamics and plasma dynamics in metals processing operations", Department of Materials Science and Engineering Massachusetts Institute of Technology (materiały nie publiowane)

6. *Blacha L.:* Hutnictwo, z. 60, Gliwice 2001

7. *Law C. N. S., Khoo B.C.:* American Institute of Chemical Engineers Journal, vol. 48, 2002, p. 1856–1868

8. *Yih S. M.:* Handbook of Heat and mass transfer, vol. 2: Mass transfer and reactor design, Gulf Publishing company, Houston, 1986

9. *Lamont J. C., Scott D.:* American Institute of Chemical Engineers Journal, vol. 16, 1970, p. 513–519

10. *Schwarze R., Savov L., Obermeier F., Janke D.:* "A numerical model flow the evaporation process of an electromagnetic stirred iron melt", European Congress on Computational Methods in Applied Sciences and Engineering ECCOMAS Computational Fluid Dynamics Conference 2001, Swansea, UK, 4–7 September 2001

11. *Kim S.-E., Choudhury D. and Patel B.:* "Computations of complex turbulent flows using the commercial code FLUENT", Proc. Symp. Modeling Complex Turb. Flows (Kluwer Academic Publishers, Dordrecht), (1999), p. 259–276

12. *Leonard B. P.:* Comput. Methods Appl. Mech., vol. 19, (1995), p. 59–98

13. *Rhie C. M., Chow W.L.:* American Institute of Aeronautics and Astronautics Journal, vol. 21, (1983), p. 1525–1232

14. *Issa R. I.:* J. Comput. Phys., vol. 62, (1986), p. 40–65